Journal of Non-Crystalline Solids 631 (2024) 122916

Contents lists available at ScienceDirect

Journal of Non-Crystalline Solids

journal homepage: www.elsevier.com/locate/jnoncrysol

Amorphous carbon nitride (C_3N_4)

Murat Durandurdu

Department of Nanotechnology Engineering, Abdullah Gül University, Kayseri, Türkiye

ARTICLE INFO

Keywords:
Carbon nitride
Amorphous
Graphite-like

ABSTRACT

This detailed investigation employs an ab initio approach to explore the atomic structure and electronic properties of an amorphous carbon nitride (C_3N_4) model. The model, designed with an exact 3:4 ratio, is based on an amorphous boron nitride configuration. The study reveals crucial insights into the mean coordination number for C and N atoms within the amorphous structure. With values of 2.95 for C atoms and 2.21 for N atoms, these coordination numbers closely resemble those observed in graphite-like crystals. The local structure of the amorphous network exhibits similarities to the triazine-based graphitic C_3N_4 crystal and is notably devoid of homopolar bonds. The estimated band gap for the amorphous C_3N_4 model is 1.2 eV, representing a significant reduction compared to the crystal structure, which exhibits a band gap of about 2.93 eV as determined through GGA+U calculations.

1. Introduction

Over the years, the exploration of various carbon nitride (CN) structures has unfolded, revealing diverse possibilities. In 1989, Liu and Cohen introduced the β-C_3N_4 structure by substituting C for Si in β-Si_3N_4 [1]. Ab initio calculations suggested its hardness to be comparable to, or even surpassing, that of diamond. Based on GW approximation, its indirect band gap was estimated to be 6.4 ± 0.5 eV [2]. Subsequently, Liu and Wentzcovitch proposed alternative structures for C_3N_4, including zinc-blende-like cubic C_3N_4 and layered graphite-like rhombohedral C_3N_4 [3]. Teter and Hemley expanded the repertoire to five structures: α-C_3N_4, β-C_3N_4, cubic-C_3N_4, pseudocubic- C_3N_4, and graphitic-C_3N_4 (g-C_3N_4) [4]. Calculations indicated that g-C_3N_4 possessed the lowest total energy.

From 1996 onward, various forms of g-C_3N_4 were investigated, with two frequently proposed structural models based on the presence of either triazine cores or heptazine (tri-s-triazine) cores [5]. Both models consist of 6-membered rings with sp^2-type bonds between C and N atoms, reminiscent of graphite. Notably, these structures inherently feature vacancies surrounded by N atoms. The presence of intrinsic vacancies and the rotational flexibility at the N—N bonding linking two building blocks, whether triazine or heptazine cores, appear to hinder the development of large-sized layers, posing challenges in achieving crystalline phases [5]. Consequently, products obtained through various synthesis processes are often reported to exhibit poor crystallinity [5].

The generation of amorphous CN samples with a C/N atomic ratio of about 3:4 was achieved through the heat treatment of partially crystalline graphitic CN, with the partial crystal structure initially possessing a bandgap of 2.82 eV [6]. The resulting amorphous variant was expected to exhibit a reduced band gap, estimated to be 1.90 eV. In this study, amorphous C_3N_4 (a-C_3N_4) was represented by a random rotation of heptazine cores. The process of homogeneous amorphization involved breaking in-plane hydrogen bonds between strands with NH/NH2 groups through annealing bulk melon [7]. A straightforward heating process, utilizing a mixture with varying mass ratios of ammonium acetate and urea in a crucible, led to the formation of amorphous CN with three-coordinate nitrogen vacancies [8]. The estimated band gap for one sample was approximately 2.58 eV. Furthermore, amorphous CN_x samples (where $x > 1$) were produced using various precursor-based methods, with proposed network structures based on cross-linked triazine units [9]. Amorphous CN powders with a C/N atomic ratio 3:4 were prepared by a solid-state reaction between cyanuric chloride or its fluoro analogue and lithium nitride [10]. The powder exhibited a graphite-like sp^2-bonded structure composed of building blocks of s-triazine rings and had a bandgap of 3.1 eV. These findings underscore the sensitivity of the electronic structure of amorphous CN to factors such as local structure, C/N ratio, impurities (H, O), etc. The intricate interplay of these elements highlights the complexity and tunability of amorphous CN's properties.

The intrinsic narrow bandgap in amorphous CN holds significant advantages, particularly in the context of photocatalysis, when compared to partially crystalline CN [11]. However, detailed atomistic-level information regarding amorphous forms remains limited, necessitating further studies to deepen our understanding of

E-mail address: murat.durandurdu@agu.edu.tr.

https://doi.org/10.1016/j.jnoncrysol.2024.122916
Received 29 January 2024; Received in revised form 25 February 2024; Accepted 7 March 2024
Available online 16 March 2024
0022-3093/© 2024 Elsevier B.V. All rights reserved.

these structures.

The conventional "melt and quench" technique, employed in standard density functional molecular dynamics approaches, faced challenges in generating amorphous CN due to the formation of numerous N—N bonds, impeding the formation of melem units [12]. As an alternative, Lu et al. adopted a method utilizing an amorphous boron nitride (BN) random network to indirectly achieve an amorphous CN configuration [12]. The resulting network demonstrated a C and N composition ratio of 1:0.98 and featured melem-type units. However, the excess of C atoms resulted in the presence of C—C bonds, and the HES06 functional indicated a band gap of 0.3 eV. In contrast, hydrogenated networks exhibited a calculated band gap close to 1.9 eV.

Building upon the methodology outlined in Ref. 12, this study replicates the generation of an a-C_3N_4 network. The resulting network consists of triazine-based g-C_3N_4, free from homopolar bonds, and exhibits a band gap of 1.2 eV, as determined through GGA+U calculations.

2. Method

In this investigation, we employed an ab initio technique grounded in the principles of density functional theory (DFT) [13]. To enhance pseudopotential contraction, the Troullier and Martins scheme was utilized [14]. For valence electrons, we adopted double zeta + polarized (DZP) basis sets, and Brillouin zone integration was carried out at the Γ point. The Perdew Burke Ernzerhof (PBE) generalized gradient approximation (GGA) [15] with Grimmer Dispersion correction [16] was employed, and a mesh grid energy cut-off of 150 Ry was implemented to determine Hartree and exchange-correlation contributions to energy.

The construction of the C_3N_4 model followed the methodology outlined in Ref.12. An initial structure of a 200-atom amorphous BN model (100 B and 100 N atoms) was utilized, where all B atoms were replaced with C atoms. Subsequent to the removal of single C or N atoms, the system underwent complete relaxation, encompassing atomic coordinates and volume, using the variable cell conjugate gradient method until the highest force reached a magnitude less than 0.01 eV/Å. This iterative process continued until achieving a stoichiometric ratio of 3:4, resulting in a final model consisting of 154 atoms (66 C and 88 N atoms). The system was then subjected to thermal equilibration at 300 K for 10.0 ps using a Nose thermostat and subsequently relaxed once more using the variable cell conjugate gradient method, employing the same force criteria as mentioned above. The crystal structure data were obtained from the Materials Project website [17]. Utilizing the lattice parameters, where $a = b = 4.78$ Å and $c = 7.08$ Å, we constructed a 112-atom crystal structure comprising 48 C and 64 N atoms. This crystal structure exhibited hexagonal symmetry (P6m2) with triazine and AB stacking. Subsequently, the structure was relaxed using the parameters and approaches described earlier.

Accurate estimation of the band gap energy for the structures was conducted through GGA+U calculations. The Hubbard potential (U) was determined by focusing on the crystal model, with $U = 8.35$ eV for the N-p state. This yielded an approximate band gap energy of about 2.93 eV for the crystal, considering the difference between the HOMO and LUMO states as the band gap. This value is consistent with literature findings ranging from 2.54 to 3.1 eV [6,18,19]. This parameter was uniformly applied across the amorphous configuration to predict its electronic structure. Partial analysis of the structures was carried out with the ISAACS program [20].

3. Results

To scrutinize the atomic arrangement disparities between the amorphous and crystalline (P6m2 with triazine and AB stacking) configurations of C_3N_4 at the atomistic level, we embarked on an analysis by examining and plotting their partial pair correlation functions (PPCFs), as illustrated in Fig. 1. Notably, the positional alignment of the first two

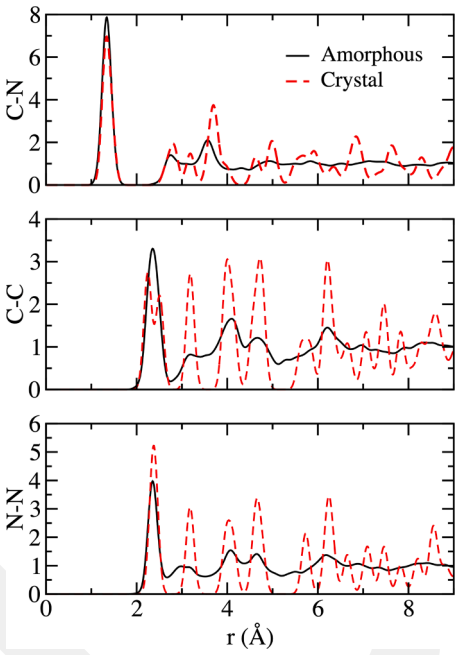

Fig. 1. Comparison of the partial pair correlation functions of amorphous and crystalline C_3N_4.

peaks in the PPCFs displayed a significant overlap for both forms of C_3N_4. This intriguing observation implies a notable similarity in their short-range and medium-range atomic arrangements. The medium-range order is likely associated with triazine units. Additionally, it is noteworthy that, akin to the graphitic crystal, the amorphous network exhibits a certain degree of chemical order.

For both the crystalline and amorphous forms, the C—N bond length measures 1.341 Å. This value is comparable to the range observed in crystalline structures, which typically falls between 1.327 Å and 1.463 Å [18]. In the case of amorphous CN, the C—N bond length is reported to be in the range of 1.30–1.43 Å [12]. The consistent C—N bond length between the amorphous and crystalline forms of C_3N_4, as well as the comparison with amorphous CN, provides insights into the structural similarities and differences among these configurations.

The mean coordination numbers, calculated with a cutoff radius of C—N = 1.97 Å, reveal distinctive characteristics of the atomic arrangement in the a-C_3N_4 structure. Specifically, the mean coordination number for C atoms is determined to be 2.95, while for N atoms, it is 2.21. These values closely align with coordination numbers of 3.0 for C and 2.25 for N in graphite-like crystals, where the fraction of threefold coordinated N is 25 %, and twofold coordinated N is 75 %. These values of the crsytal are determined using a cutoff radius of C—N = 1.93 Å.

Breaking down the specifics, around 86 % of C atoms manifest a threefold coordination, and approximately 7.5 % exhibit a twofold coordination. The remaining C atoms are found to be fourfold coordinated. On the N side, 76 % of atoms are twofold coordinated, 23 % are threefold coordinated, and there is a single N atom demonstrating onefold coordination. These statistics provide valuable insights into the local atomic environment and connectivity within the a-C_3N_4 structure. Importantly, they closely resemble the expected coordination patterns observed in graphitic crystals, contributing to a deeper understanding of the structural characteristics of the material.

The atomic structure of the amorphous configuration undergoes a more in-depth analysis through a three-body correlation function, specifically the bond angle distribution functions. C—N-C and N—C-N distributions are depicted in Fig. 2, and each displays a principal peak near 120°, signifying predominant trigonal symmetry. Additionally, the presence of a four-membered ring results in a weak peak around 85–90°, and chain-like structures produce weak peaks at large angles. This

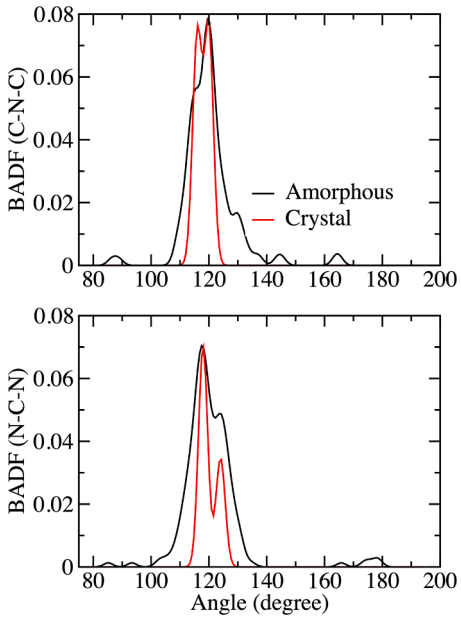

Fig. 2. Bond angle distribution of both amorphous and crystalline C_3N_4.

emphasizes the slightly diverse nature of the amorphous arrangement, showcasing variations in the bond angles within the structure. The distribution of bond angles provides valuable insights into the local geometry and connectivity of the atoms in the amorphous state.

A ring statistical analysis was conducted to gain insights into the topological connectivity of the amorphous state, and the results are presented in Fig. 3. Within the amorphous configuration, six- and twelve-membered rings are the most frequently observed. Such rings exist in triazine-based crystals, leading to the reasonable claim that the amorphous network is structurally similar to triazine-based crystals, given the prevalence of these specific ring sizes in both configurations. The analysis provides valuable information about the distribution of ring sizes, contributing to a better understanding of the topological features of the amorphous carbon nitride structure.

The electron density of states (EDOS) for both crystalline and amorphous forms of C_3N_4, calculated using the GGA+U method, is illustrated in Fig. 4, with the Fermi level shifted to zero eV. Defining the HOMO-LUMO state as a forbidden band gap, the crystal exhibits a bandgap energy of approximately 2.93 eV, aligning with previous findings in the range of 2.54–3.1 eV for the crystalline structures [6,18,19]. In contrast, the amorphous configuration presents a bandgap of about 1.2 eV. Although this value is notably lower than experimentally observed results of 1.90, 2.58 and 3.1 eV [6,8,10], it is significantly

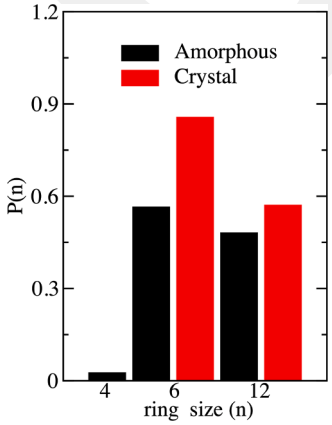

Fig. 3. Ring distribution for the amorphous and crystalline forms.

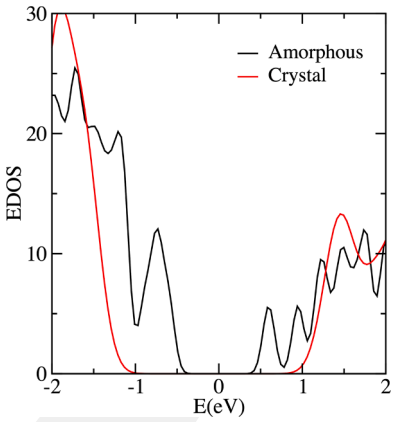

Fig. 4. The electron density of states (EDOS) for both crystalline and amorphous forms of C_3N_4, near the Fermi level, shifted to zero eV. The Gaussian smoothing factor is used to plot EDOS and hence the band gaps may appear smaller than the actual HOMO-LUMO difference.

larger than the 0.3 eV predicted using the HES06 functional [12]. It is important to note that the direct comparison of our theoretical data with experimental results provides insights into the electronic structure of amorphous CN. However, it should be acknowledged that this comparison has limitations due to the inherent structural differences between experimental samples and theoretical models. Despite these challenges, the calculated electronic properties contribute valuable information to our understanding of the amorphous C_3N_4 system.

The degree of localization of states in disordered networks is a crucial factor, and it can be characterized by the inverse participation ratio (IPR),

$$\mathrm{IPR}(\psi_j) = N\sum_{i=1}^{N} a_i^{m4} \Big/ \left(\sum_{i=1}^{N} a_i^{m2}\right)^2$$

where $\psi_m = \sum_{i=1}^{N} a_i^m \phi_i$ is the m^{th} eigenstate and N is the number of atoms. The IPR values estimated for the amorphous model are illustrated in Fig. 5. Notably, both valence and conduction states around the Fermi level (at zero eV) exhibit a considerable degree of localization, as evidenced by their high IPR values. This observation differs from early theoretical predictions, which suggested strong localization primarily in the upper valence states [12]. The discrepancy may be attributed to the distinct structural arrangements of the amorphous configurations proposed in the present and previous studies, highlighting the sensitivity of electronic states to structural details in disordered systems.

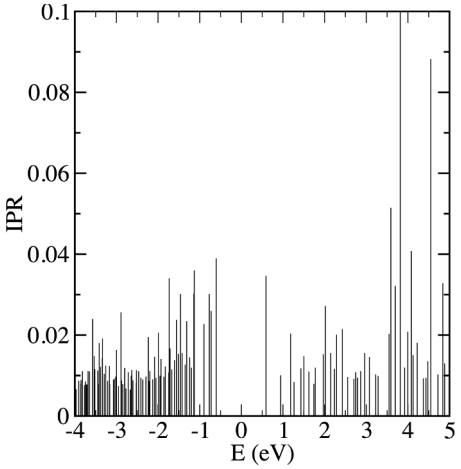

Fig. 5. Inverse participation ratio (IPR) of a-C_3N_4.

The degree of localization of states can provide valuable insights into selecting suitable types of impurities for the amorphous model. Symmetry in the localization of states suggests that shifting the Fermi energy to either the valence band or the conduction band is equally probable. Consequently, both types of doping, whether n-type or p-type, have an equal likelihood of occurrence. This symmetry in localization facilitates a balanced consideration of different doping scenarios, providing flexibility in tailoring the electronic properties of the amorphous system based on specific application requirements.

4. Conclusions

This study has delved into the intriguing realm of a-C_3N_4, uncovering its structural and electronic properties through meticulous ab initio calculations. The contracted a-C_3N_4 model, maintaining a precise 3:4 composition ratio, provides a realistic representation of this complex network. Our investigation unveils a key feature of a-C_3N_4: its close resemblance to graphite-like C_3N_4 in terms of local structure and average coordination numbers. Specifically, the mean coordination numbers for C and N atoms in our model (2.95 and 2.21, respectively) align closely with those observed in crystalline counterparts. This suggests a familiar building block – the triazine unit – plays a crucial role in both crystalline and amorphous forms. Perhaps the most captivating finding lies in the electronic realm. Our calculations reveal a significantly reduced band gap for a-C_3N_4 (1.2 eV) compared to its crystalline counterpart (2.93 eV). Our study sheds light on the fundamental nature of a-C_3N_4 but also highlights the necessity for further exploration. While the compact size and customized structural properties of the starting amorphous BN model facilitated precise composition control, proving valuable in this initial investigation, it may pose limitations in terms of generalizability. To achieve a more comprehensive understanding of this intriguing material, future studies should explore diverse starting configurations and consider larger model sizes, despite the potential challenges involved in maintaining precise composition and avoiding homopolar bonds. By broadening our scope beyond the current model, we can gain deeper insights into how the initial structural properties influence the final structure and properties of a-C_3N_4.

Declaration of generative AI and AI-assisted technologies in the writing process

During the preparation of this work the author(s) used ChatGPT and Gemini in order to improve the language. After using this tool/service, the author(s) reviewed and edited the content as needed and take(s) full responsibility for the content of the publication.

CRediT authorship contribution statement

Murat Durandurdu: Writing – review & editing, Writing – original draft, Visualization, Validation, Methodology, Investigation, Funding acquisition, Formal analysis, Conceptualization.

Declaration of competing interest

The authors declare that they have no known competing financial interests or personal relationships that could have appeared to influence the work reported in this paper.

Data availability

Data will be made available on request.

Acknowledgments

The author expresses gratitude for the support provided by the Abdullah Gül University Support Foundation. Additionally, the author acknowledges the computing resources and time generously provided by TÜBİTAK ULAKBİM High Performance and Grid Computing Center (TRUBA resources).

References

[1] A.Y. Liu, M.L. Cohen, Prediction of new low compressibility solids, Science 245 (1989) 841–842.
[2] J.L. Corkill, M.L. Cohen, Calculated quasiparticle band gap of β-C3N4, Phys. Rev. B 48 (1993) 17622–17624.
[3] A.Y. Liu, R.M. Wentzcovitch, Stability of carbon nitride solids, Phys. Rev. B 50 (1994) 10362–10365.
[4] D.M. Teter, R.J. Hemley, Low-compressibility carbon nitrides, Science 271 (1996) 53–55.
[5] M. Inagaki, T. Tsumura, T. Kinumoto, M. Toyoda, Graphitic carbon nitrides (g-C3N4) with comparative discussion to carbon materials, Carbon N Y 141 (2019) 580–607.
[6] Y. Kang, Y. Yang, L.C. Yin, X. Kang, L. Wang, G. Liu, H.M Cheng, An amorphous carbon nitride photocatalyst with greatly extended visible-light-responsive range for photocatalytic hydrogen generation, Adv. Mater. 27 (31) (2015) 4572–4577.
[7] Y. Kang, Y. Yang, L.C. Yin, X. Kang, L. Wang, G. Liu, H.M Cheng, Selective breaking of hydrogen bonds of layered carbon nitride for visible light photocatalysis, Adv. Mater. 28 (30) (2016) 6471–6477.
[8] Y. Duan, Y. Wang, L. Gan, J. Meng, Y. Feng, K. Wang, K. Zhou, C. Wang, X. Han, X. Zhou, Amorphous carbon nitride with three coordinate nitrogen (N3C) vacancies for exceptional NOx abatement in visible light, Adv. Energy Mater. 11 (19) (2021) 2004001.
[9] J.R. Holst, E.G. Gillan, From triazines to heptazines: deciphering the local structure of amorphous nitrogen-rich carbon nitride materials, J. Am. Chem. Soc. 130 (23) (2008) 7373–7379.
[10] V.N. Khabashesku, J.L. Zimmerman, J.L. Margrave, Powder synthesis and characterization of amorphous carbon nitride, Chem. Mater. 12 (11) (2000) 3264–3270. Nov 20.
[11] M.Z. Rahman, P.C. Tapping, T.W. Kee, R. Smernik, N. Spooner, J. Moffatt, Y. Tang, K. Davey, S.Z Qiao, A benchmark quantum yield for water photoreduction on amorphous carbon nitride, Adv. Funct. Mater. 27 (39) (2017) 1702384.
[12] H. Lu, Y. Guo, J.W. Martin, M. Kraft, J. Robertson, Atomic structure and electronic structure of disordered graphitic carbon nitride, Carbon N Y 147 (2019) 483–489.
[13] J.M. Soler, E. Artacho, J.D. Gale, A. García, J. Junquera, P. Ordejón, D. Sánchez-Portal, The SIESTA method for ab initio order-N materials simulation, J. Phys. Condens. Matter. 14 (11) (2002) 2745.
[14] N. Troullier, J.L. Martins, Efficient pseudopotentials for plane-wave calculations, Phys. Rev. B 43 (1991) 1993.
[15] J.P. Perdew, K. Burke, M. Ernzerhof, Generalized gradient approximation made simple, Phys. Rev. Lett. 77 (1996) 3865.
[16] S. Grimme, Semiempirical GGA-type density functional constructed with a long-range dispersion correction, J. Comput. Chem. 27 (15) (2006) 1787–1799.
[17] A. Jain, S.P. Ong, G. Hautier, W. Chen, W.D. Richards, S. Dacek, S. Cholia, D. Gunter, D. Skinner, G. Ceder, K.A. Persson, Commentary: the materials project: a materials genome approach to accelerating materials innovation, APL Mater. 1 (1) (2013).
[18] S. Datta, P. Singh, D. Jana, C.B. Chaudhuri, M.K. Harbola, D.D. Johnson, A Mookerjee, Exploring the role of electronic structure on photo-catalytic behavior of carbon-nitride polymorphs, Carbon N Y 168 (2020) 125–134.
[19] A.H. Reshak, S.A. Khan, S. Auluck, Linear and nonlinear optical properties for AA and AB stacking of carbon nitride polymorph (C_3N_4), RSC Adv. 4 (23) (2014) 11967–11974.
[20] S. Le Roux, V Petkov, ISAACS–interactive structure analysis of amorphous and crystalline systems, J. Appl. Crystallogr. 43 (2010) 81–85.